

# Photonic device design using Multiobjective Evolutionary Algorithms

Steven Manos<sup>1,2</sup>, Leon Poladian<sup>1,3</sup>, Peter Bentley<sup>4</sup>, Maryanne Large<sup>1</sup>

<sup>1</sup> Optical Fibre Technology Centre, Australian Photonics CRC, 206 National Innovation Centre, Australian Technology Park, Eveleigh NSW 1430, Australia

<sup>2</sup> School of Physics, University of Sydney, NSW 2006, Australia

<sup>3</sup> School of Mathematics and Statistics, University of Sydney, NSW 2006, Australia

<sup>4</sup> Department of Computer Science, University College London, Gower Street, London WC1E 6BT, United Kingdom  
E-mail: s.manos@oftc.usyd.edu.au

**Abstract.** The optimization and design of two different types of photonic devices - a Fibre Bragg Grating and a Microstructured Polymer Optical Fibre is presented in light of multiple conflicting objectives in both problems. The fibre grating optimization uses a fixed length real valued representation, requiring the simultaneous optimization of four objectives along with variable bounds and a single objective constraint. This led to the human selection of a Pareto-optimal design which was manufactured. The microstructured fibre design process employs a new binary encoded variable length representation. An external embryogeny, or growth process is used to guarantee the creative generation of these complex designs which are automatically valid with respect to manufacturing constraints. Some initial results are presented for the case of two objectives which relate to the bandwidth and signal loss of a design.

## 1 Introduction

As more demands are made on telecommunications and other applications of optical fibres such as sensing, demand for the complexity and functionality of these devices increases. Fibre Bragg gratings (FBG) for optical filters and switching are an inherent part of such systems, offering highly tailorable optical filtering. Microstructured Polymer Optical Fibres (MPOF) are a more recent advent in the field of photonics, promising ease of manufacture along with functionality customization. Both these areas of research are served well since they can be manufactured along with the capabilities to characterize both FBGs and MPOFs. The design of both these devices is a complicated task, and forms an excellent set of technologically relevant problems for powerful design algorithms such as Evolutionary Algorithms (EA).

The design of FBGs using EAs has previously been explored using single objective techniques [1]. Typically the design goals have been simple (for example, bandpass filters), and EAs have proven very successful. In these cases the objective function was defined as the minimisation of the difference between the

target spectrum and the design spectrum, using weights to increase the relative importance of regions of interest. The FBG used here is a 1-dimensional design problem, where the FBG features vary along the optical fibre. In this paper we consider the generalized case of multiple objectives by considering particular spectral features of interest, without reducing the problem to a single objective.

In the area of microstructured fibre design, there have been few examples of optimization technique usage. One possible reason is that the computational evaluation of traits for these types of structures can be expensive and difficult. Particular types of structures, such as hexagonal arrays of holes are used in silica due to the capillary stacking techniques used in manufacture, and this has led to most applications of microstructured fibre optimization considering these hexagonal arrays. MPOF technology on the other hand does not limit us to particular arrangements of holes, requiring the application of more general *design* techniques, as opposed to optimization using a fixed representation, which will open up the technology to more application areas. The MPOF design problem is 2-dimensional in nature, where the refractive index (placement of holes) varies across the optical fibre. In this paper we present a representation which was developed to effectively design these structures in an EA setting, along with some initial results using two conflicting objectives.

Real world engineering problems generally involve multiple objectives, and to simultaneously meet these most implementors will combine these multiple objective into a single one. In these cases, an a-priori decision is made about the relative importance of the objectives, emphasizing a particular type of solution. These techniques often require some problem-specific information, such as the total range each objective covers. In complex design problems such as those presented here, this information is rarely known in advance, making the selection of single objective weighting parameters difficult.

Instead of producing a single perfect design, multiobjective techniques consider all objectives simultaneously, resulting in a range of designs where the objectives are expressed to varying degrees (the non-dominated or *Pareto* set). Evolutionary techniques naturally lend themselves to multiobjective optimization, since they are inherently population based. Further if all the objectives can be simultaneously optimized, the whole non-dominated set converges to a single point, effectively achieving the same end results as single objective optimization.

FBGs are introduced in Section 2, along with the problem of interest and EA results in the two objective and full four objective cases. Section 3 introduces microstructured optical fibres, along with the representation used and MPOF design results.

## 2 Fibre Bragg gratings

Permanent gratings in optical fibres were first demonstrated experimentally in the late 1970's. Since then, the theoretical and experimental aspects of FBG's have flourished, resulting in a multitude of applications. FBG's have been used as stand alone devices, for example, sensing applications for strain, temperature

and voltage measurement. They have also been incorporated into fibre communications systems where they are used to combine, divide and filter digital light signals. The manufacture of FBG's has reached a level now where designs can be quickly and easily fabricated, making FBG design ideal for sophisticated design algorithms. An overview of FBG history and developments is available in [2].

The theoretical aspects of FBG's are well developed, and many *inverse* techniques to obtain a grating structure from a spectrum have been published. A recent example is presented in [3]. A common disadvantage of these methods is that the required transmission spectrum and other properties such as the group delay spectrum have to be specified over a large wavelength range. Further to that, the inverse algorithms do not allow the inclusion of other constraints, where the ability to specify important spectral features that should be present would be extremely useful. Finally, designs found using inverse techniques are often difficult to manufacture.

Experimentally, FBG's are produced by exposing a short length of optical fibre to an intense optical interference pattern, which results in a lengthwise modulation of the refractive index of the silica (glass) of the fibre. This high spatial frequency modulation is typically of the order of a  $\mu\text{m}$ , and forms an overall envelope profile which is cm's in length (Figure 1). The idea of *FBG design* is to find a profile which leads to the FBG exhibiting particular spectral properties of interest, where different wavelengths can be selectively reflected (or transmitted) to varying degrees.

Generally, the strongest interaction of the FBG with light occurs at the Bragg wavelength  $\lambda_B$ , defined by

$$\lambda_B = 2n_{\text{eff}}\Lambda \quad (1)$$

where  $n_{\text{eff}}$  is the modal effective index of the propagating wave and  $\Lambda$  is the grating period. For the purposes of this study we set  $\lambda_B = 1.55\mu\text{m}$ , but the factor  $\Lambda$  has itself previously been used as a design variable [1]. Since  $n_{\text{eff}}$  is a tunable property of the optical fibre, and  $\Lambda$  can be controlled during the grating manufacture process with relative ease, they are not included as design variables.

One of the simplest FBG's consists of a uniform grating, which leads to a sinc-function like transmission spectrum. To smooth out these side ripples in the spectrum, a tapering, or *apodization* can be introduced at each end of the grating. This process of apodization refers to gradually changing the strength of the grating, rather than an abrupt change as in a uniform FBG. In addition to that, phase changes can be introduced in the grating to induce transmission peaks in the spectrum. Various functions are used to describe this type of FBG, where we have a rolloff on the ends and a constant central region. The raised cosine  $\cos^2(z)$  is one of these commonly used functions.

## 2.1 FBG design parameters

The design parameters used in this problem are associated with details of the raised cosine function which describes the apodised profile. The most general

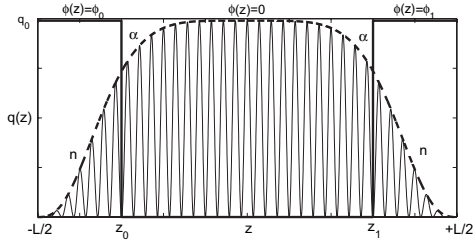


**Fig. 1.** Overview of the FBG design parameters and their contribution to various features of the profile.

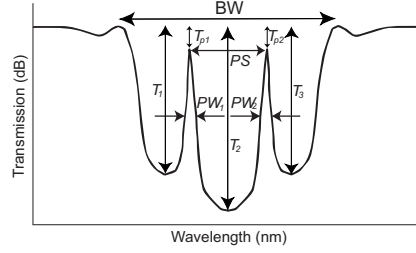


**Fig. 2.** Outline of the various spectral traits extracted using a peak-finding algorithm and used to evaluate the objectives of a design.

**Table 1.** Outline of the parameter bounds

Design parameters	Parameter bounds
Grating strength $q_0$	$0.0\text{cm}^{-1} < q_0 \leq 10.0\text{cm}^{-1}$
Total length $L$	$1.0\text{ cm} \leq L \leq 15.0\text{ cm}$
Phase $\phi_0$	$-\pi \leq \phi_0 < \pi$
Phase change positions $-z_0, z_0$	$ z_0  < L/2$
Curvatures $\alpha, n$	$1.0 < \alpha, n < 10.0$

form of the raised cosine grating structure is defined as

$$q(z) = q_0 \cos^\alpha \left( \frac{\pi}{2} \left| \frac{2z}{L} \right|^n \right) e^{i\phi(z)} \quad (2)$$

where  $\phi(z)$  describes the phase over the length of the grating.

The function itself contains four design parameters:  $q_0$  is the peak strength of the grating,  $L$  is the total length of the grating,  $n$  controls the curvature of the end drops and  $\alpha$  controls the curvature of the ends. Typically  $\alpha = 2$ , but can be generalized to other values. The phase  $\phi(z)$  can consist of a single or multiple steps. In the case where there are constant phase changes on each end of the grating, we have that  $\phi(z) = \phi_0$  for  $z < z_0$ ,  $\phi(z) = \phi_1$  for  $z > z_1$ , otherwise  $\phi(z) = 0$ , where  $z_0$  and  $z_1$  are the locations of the  $\phi_0, \phi_1$  phase changes.

In the most general case where all the above parameters are free design variables, we have a search space of 9 dimensions. In this study we make the design symmetrical about  $z = 0$  by imposing  $\phi_0 = \phi_1$  and  $z_0 = -z_1$ . The contribution of these parameters to the FBG design is shown graphically in Figure 1. The spectrum of the FBG was evaluated using the transfer matrix method.

## 2.2 FBG design objectives

The spectral characteristics of interest relate to the extraction of OTDM (Optical Time Domain Multiplexing) signals from a data stream. Further details on this are available in [4] [5].  $T_1, T_2, T_3$  are the depths of the three transmission dips,  $BW$  is the overall bandwidth,  $PS$  is the spacing of the two transmission peaks and  $PW_1$  and  $PW_2$  are their respective peaks widths, as shown in Figure 2. These spectral traits were combined into the following four objectives:

- 1. Minimization of signal interference** by minimizing the maximum (worst) of  $T_1, T_2, T_3$ . Objective 1  $\rightarrow \min(\max(T_1, T_2, T_3))$ .
- 2. Target bandwidth of 1nm.** Objective 2  $\rightarrow \min |1.0 - BW|$ .
- 3. Target peak separation of 0.08nm** for optimal extraction of the OTDM 10GHz clock signal. Objective 3  $\rightarrow \min |0.08 - PS|$ .
- 4. Increasing signal clarity** by minimizing the worst (largest) full width half maximum peak width. Objective 4  $\rightarrow \min(\max(PW_1, PW_2))$ .

We refer to these objectives for the remainder of the paper as  $T, BW, PS$  and  $PW$  respectively. An inequality constraint was also included to allow the consideration only of designs which had minimal signal loss (better than  $-0.5\text{dB}$ ) from the two central transmission peaks, such that  $\min(T_{p1}, T_{p2}) + 0.5 \geq 0$ .

## 2.3 Application of the multiobjective Evolutionary Algorithm

The Non-Dominated Sorting Genetic Algorithm (NSGAI) [6] was used as the selection mechanism, as it firstly provides an efficient method of elitist sorting and results in a well-spread final non-dominated set. Secondly, no external parameters need to be defined or tested. The 6 real valued design parameters used were bounded (Table 1), taking into consideration practical manufacturing limitations, such as the minimum length ( $L_{min}=1\text{cm}$ ) and maximum grating strength ( $q_{0max}=10\text{cm}^{-1}$ ). Simulated binary crossover (SBX) was used along with the polynomial mutation operator [7], and the design parameter bounds were enforced within these operators: any violations were simply repaired by setting them to the minimum or maximum bounds. A population size of 100, crossover probability of  $p_c = 0.9$ , mutation probability of  $p_m = 0.2$  and random initial populations were used throughout.

The constraint defined in the previous section was dealt with by altering the definition of *domination*, which is used when sorting individuals according to their non-dominated level and deciding winners during tournament selection. Design **a** dominates **b** if any of the following are true

- **a** and **b** are infeasible, but **a** has a smaller constraint violation ( $\mathbf{a}_c > \mathbf{b}_c$ )
- **a** is feasible ( $\mathbf{a}_c \geq 0$ ) and **b** is not ( $\mathbf{b}_c < 0$ )
- **a** and **b** are feasible and **a** dominates **b** in the usual Pareto-optimal sense

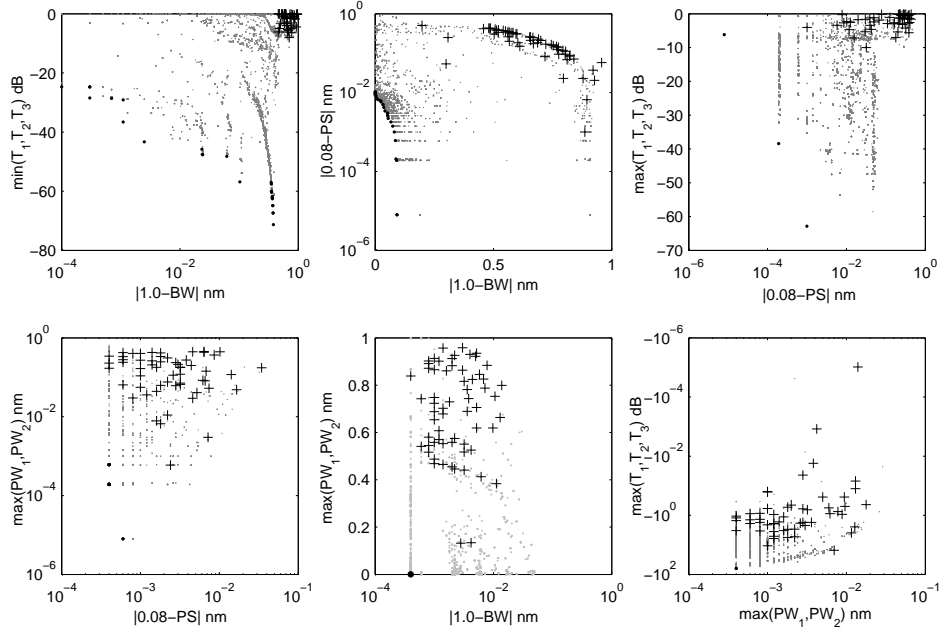


**Fig. 3.** All pairings of the 4 objectives outlined in Table 2. Crosses indicate the initial population, light grey points show all designs produced which satisfy the constraint, and the black points indicate the final non-dominated set after 100 generations.

## 2.4 FBG optimization results

Bi-objective design is one of the most widely studied problems in multiobjective optimization. Given our objective space of 4-dimensions, along with unknown relationships between the objectives, a simpler bi-objective methodology was firstly used. A recent publication [8] examined the issue of high numbers of objectives through the examination of pair-wise objective relationships. Objectives can be classified into harmonious and conflicting pairs. If a pairing is harmonious, which other objective suffers as a result, or do some objectives naturally follow and also improve? From these paired results we can also get some idea of the intrinsic dimensionality of the four objective non-dominated set. All 6 possible pairings were optimized over 100 generations, which was found sufficient to obtain a general idea of the non-dominated set. The SBX operator spread index  $\eta_c = 5$  and polynomial mutation operator spread parameter  $\eta_m = 10$  were used to facilitate a coarse parameter search. The results are shown in Figure 3, and the relationships summarized in Table 2. The most conflicting relationship was for the  $(BW, T)$  pairing, to a lesser degree followed by the  $(BW, PS)$ ,  $(PS, T)$  and  $(PS, PW)$  pairings. The final two pairings  $(BW, PW)$  and  $(T, PW)$  were harmonious, but in the process of optimizing for these objectives simultaneously, the other two objectives - respectively  $T, PS$  and  $PS, BW$  suffered. This indi-

**Table 2.** Summary of conflict and harmony in the 6 pairwise objectives.

Objective 1	Objective 2	Type	Worst objectives
<i>BW</i>	<i>T</i>	Conflicting	-
<i>BW</i>	<i>PS</i>	Conflicting	-
<i>PS</i>	<i>T</i>	Conflicting	-
<i>PS</i>	<i>PW</i>	Conflicting	-
<i>BW</i>	<i>PW</i>	Harmonious	<i>T, PS</i>
<i>PW</i>	<i>T</i>	Harmonious	<i>BW, PS</i>

cates that there will be a non-dominated relationship when considering all four objectives simultaneously, resulting in a non-dominated set manifold where most of the variance exists in 2-dimensions as a result of the strongest conflict between *BW* and *T*.

The full 4 objective problem was then run for 1000 generations using a population size of 100,  $\eta_c = 5$  and  $\eta_m = 10$ . The evolution of the design parameter space from the initial random population to the final non-dominated set is shown in Figure 4. To aid in the visualisation of the final non-dominated set, the ISOMAP [9] algorithm was used to reduce the dimensionality of the data. It was found that most of the variance (92%) was due to a 2-dimensional non-linear manifold embedded in the 4-dimensional space. Principle Component Analysis (PCA) was also attempted, but did not effectively realize the relationships between points due to their non-linear nature. The arrangement of non-dominated points on this 2-dimensional manifold is shown in Figure 5. Two clusters of points are evident. Cluster A consists of designs which all excel in the *PW* objective, and mainly vary in terms of the three remaining objectives. Cluster B on the other hand contains designs with good *BW* which mainly vary in terms of the harmonious objectives *PW* and *T* but have good *BW*. As the transmission objective gets better from bottom to top, so does the peak width. This cluster is *locally non-dominated* due to the conflicting relationship between the *BW, T* and *BW, PS* pairings. In terms of the parameters, the designs in clusters A and B all converged to values of approximately  $\phi = +\pi$ ,  $\alpha = 1.0$ , and  $z_0 = 0.1\text{cm}$ . The main variation overall occurs in the curvature  $n$ . In some runs they also converged to  $\phi = -\pi$ . The constraint handling method proved particularly efficient, since within a few generations only FBG designs within the constraint bounds were being produced.

Even though all of the designs in Figure 5 have good objectives to varying degrees, the two clusters represent two distinct types of FBGs found. Cluster A consists of longer but weaker gratings, whereas cluster B consists of shorter but stronger gratings (reflected in the groupings seen in Figure 4). As decision makers, we become more interested in cluster B since the second trough is wider, facilitating better signal quality. A Pareto-optimal FBG design with a good balance of objectives was chosen for manufacture. The FBG profile, theoretical

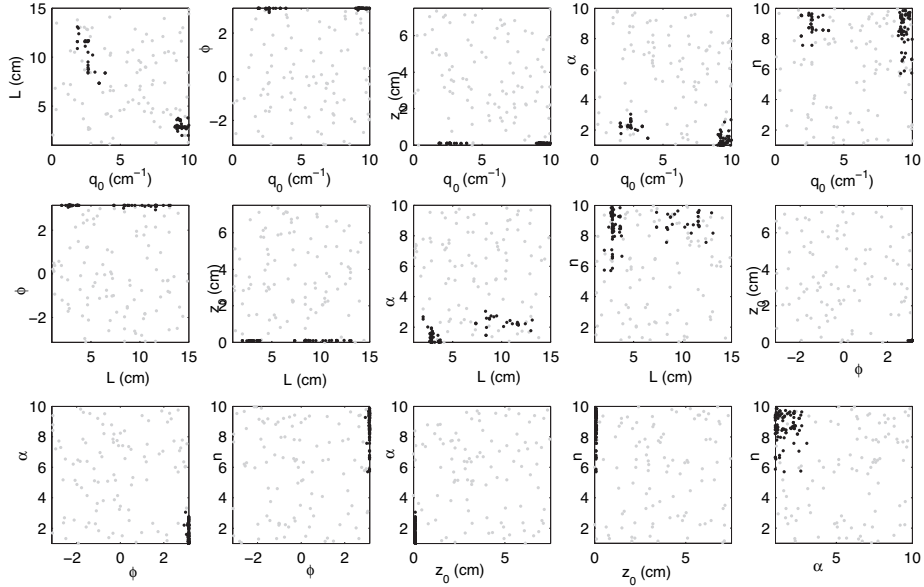


**Fig. 4.** Scatterplots in parameter space for the 4 objective FBG optimization problem. Light grey dots indicate the initial population, and black dots indicate the final non-dominated set after 1000 generations.

spectrum and experimental spectrum are shown in Figure 6. Further work will involve the manufacture and testing of other Pareto-optimal designs.

### 3 Microstructured optical fibres

Most optical fibres in use today are made of glass (silica) with solid cores. Deposited chemicals inside the core alter the refractive index profile of the glass and therefore its light guiding properties. Some previous work focused on the single objective optimization of such a fibre [10]. In recent years, silica holey fibres, or Photonic Crystal Fibres (PCF), which use air holes that run the length of the fibre, have presented themselves as an exciting new development in photonic technology. Even more recently has been the development of holey fibres in polymer - Microstructured Polymer Optical Fibres (MPOF), allowing the cheap and easy fabrication of arbitrary hole patterns in fibres. An overview of the technology is given in [11].

The refractive index profile in microstructured fibres is 2-dimensional - increasing the design complexity immensely. Many examples of holey fibres have so far focussed on arrangements of holes which relate to the manufacturing process, such as the stacking of capillaries in silica fibres which produce hexagonal array type structures. This has also been the basis of the numerical optimization of these structures - since the design can easily be parametrized into a relatively

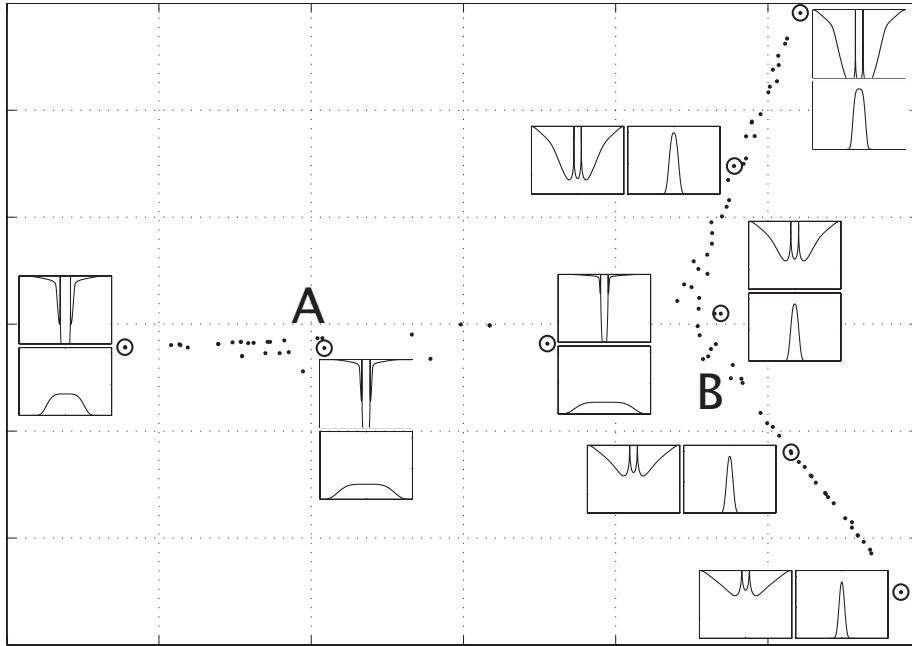


**Fig. 5.** Non-dominated designs of the four objective FBG problem represented as a flattened-out two dimensional surface. Two main clusters of designs, A and B are evident. Some of the designs (circled) have their spectra and FBG profile shown. Axes have been removed for clarity, and the plot bounds are: FBG spectrum -  $\lambda \rightarrow [1549.5, 1550.5]\text{nm}$ ,  $T \rightarrow [-70, 0]\text{dB}$ , and FBG profile -  $L \rightarrow [-5, 5]\text{cm}$ ,  $q_0 \rightarrow [0, 11]\text{cm}^{-1}$ .

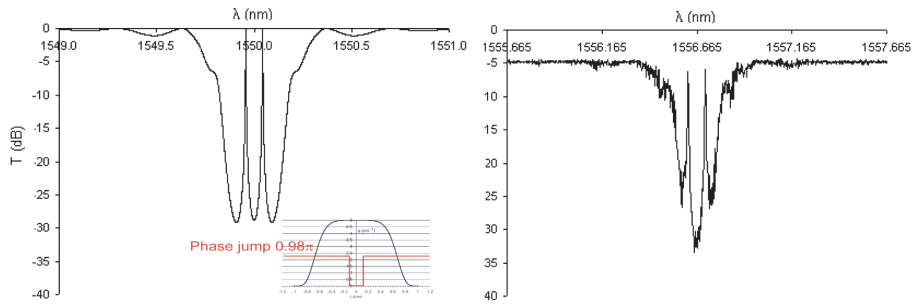


**Fig. 6.** **Left:** Theoretical spectrum from the Pareto optimal FBG shown in inset. **Right:** experimental spectrum of the manufactured FBG.

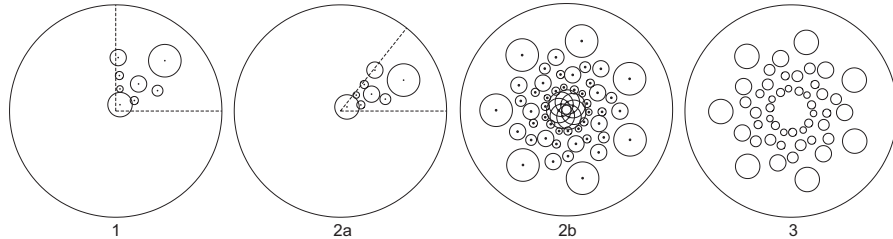
small search space [12]. But what about the *generic design* of such structures - where no pre-disposition is to be made about the arrangement of holes? This is important given the large space of designs that can be manufactured using MPOF technology, for various applications from sensing to data transmission. We are no longer limited as much in terms of the creativity of designs, thus generic design sits very well with the MPOF technology.

Some of the recent fibre development work has focussed on the application of MPOF to high bandwidth data transmission applications. This section of the paper presents some initial work in using genetic algorithms to design such generic structures in a multiobjective setting.

### 3.1 Representation

Given the complexity of microstructured fibres - especially when considering in parallel constraints such as holes not overlapping and also conforming to manufacturing constraints (minimum wall thickness between holes), a flexible representation needs to be found. A general scheme was devised which can describe arbitrary hole patterns, automatically conforming to manufacturing constraints imposed through the use of an embryogeny, where the fibres are grown. The only hard constraints built into the representation is that some symmetry  $n_{symm} \geq 2$  is imposed, and that structures consist entirely of holes.

The process of the binary genotype  $\rightarrow$  phenotype (holey fibre structure) conversion is outlined below.



**Step 1. The binary genotype is decoded into the symmetry  $n_{symm}$ , and  $N_h$  triplets of  $x_i, y_i, r_i$  values.** The triplets describe the placement of holes in the first sector of the  $x, y$  plane, forming the raw structure with  $n_{symm} = 4$ . The binary versions of  $x_i, y_i$  are decoded to the real valued position of the hole.  $r_i$  is decoded to an integer value: each possible value refers to a user defined list of available hole sizes, which reflect the available drills used to produce the initial MPOF preform.

**Step 2. The  $N_h$  hole positions  $x_i, y_i$  are symmetrized into the new symmetry  $n_{symm}$**  (a symmetry of 7 is used in the above example). **2a.** The holes are converted to polar coordinates  $r_i, \theta_i$ , where  $\theta_i$  values are scaled by

$n_{\text{symm}}/4$ . **2b.**  $(n_{\text{symm}} - 1)$  copies of the holes are made to complete the fibre.

**Step 3. The holes are grown until manufacturing constraints prohibit further growth.** We start with all holes having zero radius. The holes are grown in a step wise manner through the list of available hole sizes, and stop growing when they are within  $w_h$  of a neighboring hole or exceed their own maximum radius  $r_i$ . Growth states are updated in parallel at the end of every hole growth cycle, and the cycle is terminated when the growth state of every hole is false.

We can see that some holes are not influenced at all by surrounding holes, reaching the maximum allowed radius encoded in their genotype. Other holes never grow at all, but lay dormant in the genotype to appear in later generations during the evolutionary process. Most holes grow until inhibited by the surrounding phenotype. The advantage of using a growth scheme during the genotype  $\rightarrow$  phenotype conversion is clear - we always automatically obtain manufacturable designs without the need for a penalty function or other constraint handling techniques. Each hole is of a size that can be inserted into the polymer, and the minimum wall thickness between holes guarantees structural stability.

### 3.2 Recombination and mutation operators

Single point crossover is used, where the crossover of two parents results in a single child being generated. Firstly a random point is chosen on parent 1. This in turn sets a constraint as to the selection of the crossover point in parent 2 since we have to preserve the length of the  $n_{\text{symm}}$  and hole  $x_i, y_i, r_i$  gene segments. Using this type of crossover, children often share the characteristics of the parents, and may become simpler or more complex structures depending on the two crossover locations.

Binary mutation with a probability of  $p_m = 0.0035$  is used to mutate the binary strings. Two other types of mutation are also used -  $p_a = 0.003$  refers to the frequency of hole addition to an individual, and  $p_d = 0.003$  refers to the probability of hole deletion. No testing of different  $p_m, p_d, p_a$  values has currently been done to ascertain the best values to use for this type of representation.

### 3.3 MPOF design objectives

Two of the most important performance measures for transmission fibres relate to bandwidth and transmission loss [13]. Both of these parameters are computationally expensive to evaluate, but some approximations can be made.

**Bandwidth.** Polymer based fibres are typically highly multimodal, and a good approximation to bandwidth can be defined in terms of the fastest and slowest propagating modes in the fibre. Reducing this difference in velocity between these two extreme modes increases the bandwidth since adjacent light pulses in the fibre don't interfere as they spread while traveling down the fibre. Using a parabolic refractive index across the fibre approximately equalizes these mode

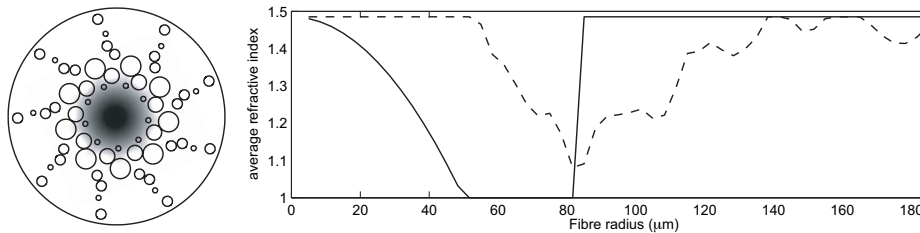


**Fig. 7.** **Left:** Randomly generated fibre design with the core fundamental mode field  $|\psi_{01}|$  overlaid (graded region on the centre of the fibre), with  $\gamma = 2.02 \times 10^{-6}$ . **Right:** The solid line indicates the target average fibre profile, and the dashed line shows the average profile of the design to the left. The average profile objective is 0.14.

velocities, effectively increasing the bandwidth. To apply this argument to holey fibres, small holes in the fibre microstructure are not completely resolved by the light, and we can approximate the whole structure by an averaged refractive index profile. So we can increase the bandwidth in a design by best suiting the average of the hole arrangement to a parabolic profile  $n(r) = 1.48 - \alpha r^g$ , where 1.48 is the refractive index of PMMA polymer at the wavelength  $\lambda = 0.833\mu\text{m}$  and  $g = 2$ . A small area of minimal refractive index ( $n = 1.0$ ) is added to the outside of the core to help increase light confinement. The objective is to then minimize the mean difference between the target profile and the design average profile. The average profile of a randomly generated design is shown in Figure 7.

**Transmission loss** in MPOFs can be attributed, amongst other things, to material absorption and scattering due to surface roughness [13]. Material absorption in the polymer is well known and can be quantified. Scattering from surface roughness on a microscopic scale arises during the manufacture of the fibre preform, when holes are drilled into the polymer using a computer numerically controlled (CNC) mill. As light travels down the fibre, the interaction of the light with air-polymer interface of the holes results in the light scattering and coupling to lossy cladding modes, reducing signal intensity. A complete numerical evaluation of this overall loss is computationally expensive, but a simple approximation is to consider the overlap of the (normalized) fundamental mode  $\psi_{01}$  with the air-polymer interfaces. Reducing this overlap

$$\gamma = \sum_{i=1}^{N_h} \oint_{h_i} |\psi_{01}|^2 r_i d\theta \quad (3)$$

effectively reduces the interaction of light with the air-polymer interface. Here  $N_h$  is the number of holes and  $r_i$  is the radius of hole  $h_i$ . The mode is evaluated at the wavelength  $\lambda = 0.833\mu\text{m}$ . A numerical algorithm based on the Fourier decomposition method was used to solve Maxwell's scalar wave equation for the generated fibre structures. This particular implementation [14] was used since it has the ability to quickly evaluate the mode profiles of arbitrary MPOF

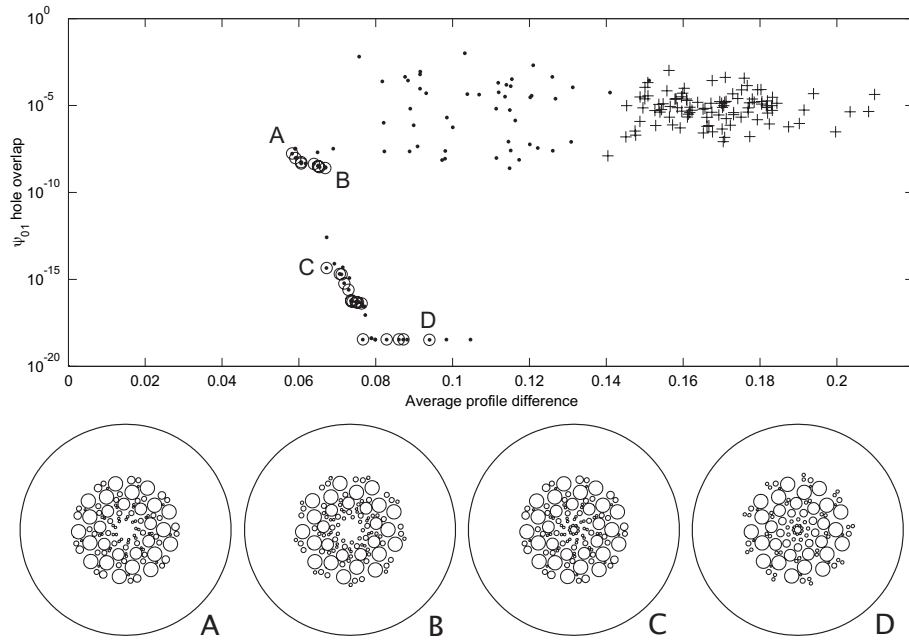


**Fig. 8. Top:** Population evolution with respect to the 2 design objectives. Crosses indicate the initial population, black dots the final population after 5000 generations and circles the final non-dominated set. **Bottom:** Four designs from the final non-dominated set, A,B,C and D are shown.

structures, thus allowing complete automation for effective use in an evolutionary algorithm. An example of a fundamental mode is shown as a shaded region in the centre of the fibre in Figure 7.

### 3.4 MPOF design

A random population of size 100 was used along with the NSGAI algorithm to order designs for subsequent selection into the next generation. Tournament selection ( $k = 2$ ) was used to compare individuals for breeding based on their non-dominated levels and crowding distance measure. The algorithm was run over 5000 generations. The objective value calculations are computationally expensive, and for a run this long some parallelization was implemented. On shared memory architectures, OpenMP allows for trivial speedup given an objective evaluation loop. For example, in our C++ code it was achieved as follows:

```
#include <omp.h>
...
int i, popnsize = popn.size();
#pragma omp parallel default(shared) private(i)
{
```

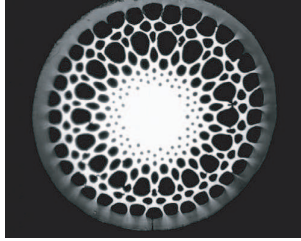


**Fig. 9.** Example of a fabricated MPOF with an average parabolic profile. The outer diameter of the fibre is approximately  $220\mu\text{m}$ .

```

#pragma omp for schedule(dynamic)
for(i=0; i<popnsize; i++)
    popn[i].evaluate_objectives();
}

```

Figure 8 shows the evolution from the initial random population to the final non-dominated set of designs. A good range of fibres are discovered. For example, A has a very good average index profile close to a parabolic index variation (0.0582) but the worst field hole overlap in the non-dominated set ( $1.7 \times 10^{-8}$ ). Design D is the other extremal solution, with an average index profile objective value of 0.094 but a very minimal overlap value of  $3.32 \times 10^{-19}$ . This is caused by the confining ring of small holes in the central region, which simultaneously conflict with the average index objective by not gradually changing the average index. Designs B and C are intermediates on the non-dominated set, with objective values of  $[0.0669, 2.61 \times 10^{-9}]$  and  $[0.0672, 4.5 \times 10^{-15}]$  respectively.

An example of a manufactured MPOF with a good parabolic average index profile is shown in Figure 9. This particular design was not evolved using the EA discussed, but demonstrates the feasibility of manufacturing these designs. This MPOF design work is still in its initial stages. Future research will include the manufacture of these evolved MPOFs, followed by the experimental characterization of the bandwidth and loss associated with the objectives used.

## 4 Conclusion

In this paper we have demonstrated the successful application of evolutionary multiobjective algorithms to two quite different photonic design problems. Through the use of real parameter optimization we were able to identify Pareto-optimal FBGs, and choose a suitable design with a good balance of properties for manufacture. A more generic design approach to MPOFs demonstrated the effectiveness of a powerful and expressive representation along with EMO techniques to design complicated microstructured fibres. The creativeness of the evolutionary process went hand in hand with the breadth of manufacturable MPOF designs. Both these areas of design are still in early stages, where future work will involve fabrication and experimental characterization of evolved designs.

**Acknowledgements** The authors would like to acknowledge the computational resources of Australian Centre for Advanced Computing and Communications ( $AC^3$ ) and Sydney Vislab, Brian Ashton for the fibre Bragg grating manufacture, the Bandwidth Foundary, the Microstructured Polymer Optical Fibre research group at the Optical Fibre Technology Centre and helpful discussions with Professor Kalyanmoy Deb and Santosh Tirawi of the Kanpur Genetic Algorithms Laboratory.

## References

1. Cormier, G., Boudreau, R.: Read-coded genetic algorithm for bragg grating parameter synthesis. *Journal of the Optical Society of America, B* **18** (2001) 1771–1776
2. Hill, K.O., Meltz, G.: Fibre bragg grating technology fundamentals and overview. *Journal of Lightwave Technology* **15** (1997)
3. Poladian, L.: A simple gratings synthesis algorithm. *Optics Letters* **25** (2000) 787–789
4. Attygalle, M., Ashton, B., Nirmalathas, A., Poladian, L., Padden, W.: Novel technique for all-optical clock extraction using fibre bragg gratings. In: *OptoElectronics and Communications Conference, Shanghai, China.* (2003) 13–16
5. Manos, S., Poladian, L., Ashton, B.: Novel fibre bragg grating design using multiobjective evolutionary algorithms. In: *CLEO/IQEC, San Francisco, California, USA.* (2004)
6. Deb, K., Pratap, A., Agarwal, S., Meyarivan, T.: A fast and elitist multiobjective genetic algorithm: NSGA-II. *IEEE Transactions on Evolutionary Computation* **6** (2002) 182–197
7. Deb, K., Beyer, H.: Self-adaptive genetic algorithms with simulated binary crossover. *Evolutionary Computation Journal* **2** (2001) 197–221
8. Purshouse, R.C., Fleming, P.J.: Conflict, harmony and independence: Relationships in evolutionary multi-criterion optimisation. In: *Proceedings of the Second International conference on Evolutionary Multi-Criterion Optimization (EMO).* (2003) 16–30
9. Tenenbaum, J.B., de Silva, V., Langford, J.C.: A global geometric framework for nonlinear dimensionality reduction. *Science* **290** (2000) 2319–2323
10. Manos, S., Poladian, L.: Optical fibre design using evolutionary strategies. *Engineering Computations* **21** (2004) 564–576
11. van Eijkelenborg, M., Argyros, A., Barton, G., Bassett, I., Fellow, M., Henry, G., Issa, N., Large, M., Manos, S., Padden, W., Poladian, L., Zagari, J.: Recent progress in microstructured polymer optical fibre fabrication and characterization. *Optical Fiber Technology* **9** (2003) 199–209
12. Manos, S., Mitchell, A., Lech, M., Poladian, L.: Automatic synthesis of microstructured holey fibre designs using numerical optimisation. In: *Australian Conference on Fibre Optic Technology (ACOFOT), Sydney Convection Centre, Darling Harbour, Sydney, Australia.* (2002)
13. Barton, G., van Eijkelenborg, M., Henry, G., Issa, N., Klein, K.F., Large, M., Manos, S., Padden, W., Pok, W., Poladian, L.: Characteristics of multimode microstructured pof performance. In: *Plastic Optical Fibre (POF) Conference, Seattle, USA.* (2003) 81–84
14. Poladian, L., Issa, N.A., Monro, T.: Fourier decomposition algorithm for leaky modes of fibres with arbitrary geometry. *Optics Express* **10** (2002) 449–454